Effect of Particle Size Distribution and Occupied Area of CdS Photosensitizers on Their Photovoltaic Performance

B. Yarmand*

Department of Nanotechnology and Advance Materials, Materials and Energy Research Center, Karaj, Iran

ABSTRACT

Cadmium sulfide (CdS) photosensitizers were successfully formed on the mesoporous titania films using the successive ionic layer adsorption and reaction (SILAR) method in five cycles, and the effects of particles size distribution and their occupied surface area on the morphology, topography, optical property, and photovoltaic performance were investigated. Scanning electron microscope (SEM) images demonstrated that the increase in the number of SILAR cycles increased the number of deposited particles as well as their sizes so that the surface morphology after the third SILAR cycle changed from non-uniform particles to a uniform layer. The surface topography of all layers was hill-valley like, the roughness of which decreased as homogeneous layers formed. The absorbance spectra measured by UV-Vis spectrophotometer revealed that the absorbance spectra of the films increased and shifted towards longer wavelengths as the number of SILAR cycles increased, which is due to the increase in the particles size distribution. Photovoltaic measurements clarified that increase in the particles size distribution had the dominant effect up to the third SILAR cycle and increased the power conversion efficiency to a maximum of 4.65 %. However, as the occupied surface area increased due to the extreme formation of CdS particles and blocking of porosities in the mesoporous titania film, the efficiency dropped to 2.64 %.

1. INTRODUCTION

An obstacle to the development of solar cells is their low power conversion efficiency due to inability to harvest the full solar spectrum. Various approaches have been proposed to enhance the light absorption of solar cells, the most important of which is multi-junction solar cells. In multi-junction solar cells layered structure that usually consist of three layers are used. The upper, the middle and the lower layers absorb photons with high (ultraviolet region), average (visible region) and low (infrared region) energy levels, respectively. Although these cells exhibit the highest power conversion efficiency as they absorb most of the incident photons, their complicated manufacturing process and their high production costs have prevented their commercialization [1-3].

In recent years, a novel approach has attracted the attention of researchers in which chalcogenide semiconductors are used as photosensitizers to extend the absorption spectrum of the incident photons. This is because the energy gap of chalcogenide semiconductor photosensitizers can be tuned by controlling their sizes; as a result of this, the absorption spectrum can be adjusted to match the spectral distribution of the sun. Chalcogenide semiconductor photosensitizers have large extinction coefficients due to the quantum confinement effects. Moreover, these photosensitizers have large intrinsic dipole moments, which may lead to a rapid charge separation [4-6].

In addition to maximum absorption of incident photons as well as electron injection to based photoanode material's conduction band, an ideal photosensitizer should have the minimum interference with the performance of the solar cell. The absorption level of chalcogenide semiconductor photosensitizers is a function of particle size, which can be maximized by implementing a wide distribution of different particle sizes. The most significant weakness of this type of photosensitizers is associated with the occupied surface area of particles as it deactivates part of the photoanode surface. Achieving maximum power conversion efficiency of a solar cell sensitized with semiconductor nanoparticles requires optimization of these two factors [7-10]. So far, the effect of different compounds such as PbS, PbSe, CdS and CdSe on the efficiency of solid state and photoelectrochemical solar cells have been

*Corresponding Author's Email: byarmand@merc.ac.ir (B. Yarmand)

investigated. The results indicate that CdS has been the most effective due to its suitable band gap, long life, excellent stability, and easy fabrication [11-15].

Amongst the physical and chemical methods used for deposition of semiconductor nanoparticles, the best way for in situ formation of CdS is the simple and low cost process of successive ionic layer adsorption and reaction (SILAR) which enables a precise control over the nucleation and growth of nanoparticles. SILAR method involves the adsorption of a Cd^{2+} precursor on the surface and subsequently, its reaction with a S^{2-} precursor, which leads to the formation of CdS on surface [16-18].

Considering the significant effects of such factors as particles size distribution and occupied area of the photosensitizer on the performance of solar cells, they were simultaneously investigated in the present study. For this purpose, photoelectrochemical cells were prepared through deposition of CdS photosensitizers on the mesoporous titania film using the SILAR method, and changes in their morphology, topography, optical property and photovoltaic performance were evaluated during different cycles. Different morphologies, ranging from particle to continuous layer, can be produced by changing the number of cycles in the SILAR method.

2. MATERILAS AND METHOD

2.1. Preparation and sensitization of photoanode

Titania photoanodes with mesoporous structure were prepared by sol-gel templating technique. 5 g of titanium tetraisopropoxide (Merck) was hydrolyzed using 3.2 g of hydrochloric acid (Merck) under stirring for 10 min. The hydrolyzed sol was mixed with 1 g of Pluronic P123 (Aldrich) surfactant dissolved in 21 g of ethanol (Merck). Subsequently, FTO substrates with sheet resistance of 10 Ω⁄sq (Solaronix) were coated with spin coater at 2000 rpm for 30 s. The films were then aged at 10 °C for 24 h under controlled humidity of 65-75 %. The samples were finally annealed in a tube furnace at 400 °C for 1 h under air with a heating rate of 1 °C/min. The films were thickened about 5 μm after ten deposition cycles.

Photoanodes were initially in situ sensitized by CdS photosensitizer grown by SILAR processes. Photoanodes were successively immersed in two different solutions for 5 min each, first in aqueous solution containing 0.5 M $Cd(NO_3)_2$ and then in thiourea aqueous solution at 50 °C. Following each immersion, the photoanodes were rinsed with water and then were dried. All these processes are termed as one SILAR cycle and repeated five cycles. After that, photoanodes were immersed in 0.5 mM ethanolic solution of *cis*-diisothiocyanato-bis(2,2'-bipyridyl-4,4'-dicarboxylato) ruthenium(II) bis(tetrabutylammonium) (N719, Solaronix) and kept at room temperature for 72

h. The dye-adsorbed photoanode was then rinsed thoroughly with ethanol and subsequently dried.

2.2. Fabrication of photoelectrochemical cell

The counter electrode were prepared by spreading a drop of 10 mM H_2PtCl_6 (Merck) in isopropanol (Merck) on FTO substrate and heating it to 400 °C for 15 min under air ambient. The polysulfide electrolyte prepared freshly by dissolving 0.5 M Na_2S (Merck), 0.2 M sulfur (Merck), and 0.2 M KCl (Merck) in ultrapure water/methanol (7:3 by volume). After that, the sensitized photoanode and counter electrode were assembled into a sandwich type cell and sealed by 25 μm thick thermoplast hot-melting sealing foil (SX 1170-25, Solaronix). The electrolyte was injected into the cell by capillary forces through a hole drilled in the counter electrode. The hole was covered and sealed with a quickly solidifying epoxy polymer to prevent fluid-type electrolyte leakage. The cells had an active area of 0.25 cm^2.

2.3. Characterization and measurments

The morphology and surface relief of the prepared photosensitizers were observed using scanning electron microscope (SEM, 360, Cambridge) and atomic force microscope (AFM, CP, Auto probe), respectively. The optical absorbance spectra of the films were recorded using a UV-Vis spectrophotometer (Lambda 25, Perkin Elmer) with a scanning rate of 60 nm/min in the wavelength range of 300 − 800 nm. Photovoltaic measurements were performed under 1 sun AM 1.5G simulated sun light using a solar simulator (luzchem) and a potentiostate/galvanostae (PGSTAT 302N, Autolab, Eco-Chemie).

3. RESULT AND DISCUSSION

3.1. Microstructure
Fig. 1 shows the surface of the CdS sensitized titania films after different SILAR cycles. It could be seen that after the first SILAR cycle, CdS particles of different sizes and shapes are non-uniformly distributed and formed on the titania films, where areas of aggregated as well as sparse particles could be observed. After the second SILAR cycle, more CdS particles are formed compared to the first cycle, resulting in a decreased sparse particle area. The size range of these nanoparticles is wider than the previous cycle which is due to the better growth of the formed nanoparticles in the first SILAR cycle compared with the second SILAR cycle. This is because the surface of the formed particles in the initial cycles is a preferred site for adsorption of ions and their reaction in the following cycles. As it could be seen, after the third SILAR cycle, the number and size of CdS particles increase, which results in their collision and consequently the formation of a continuous porous cover all over the titania surface.
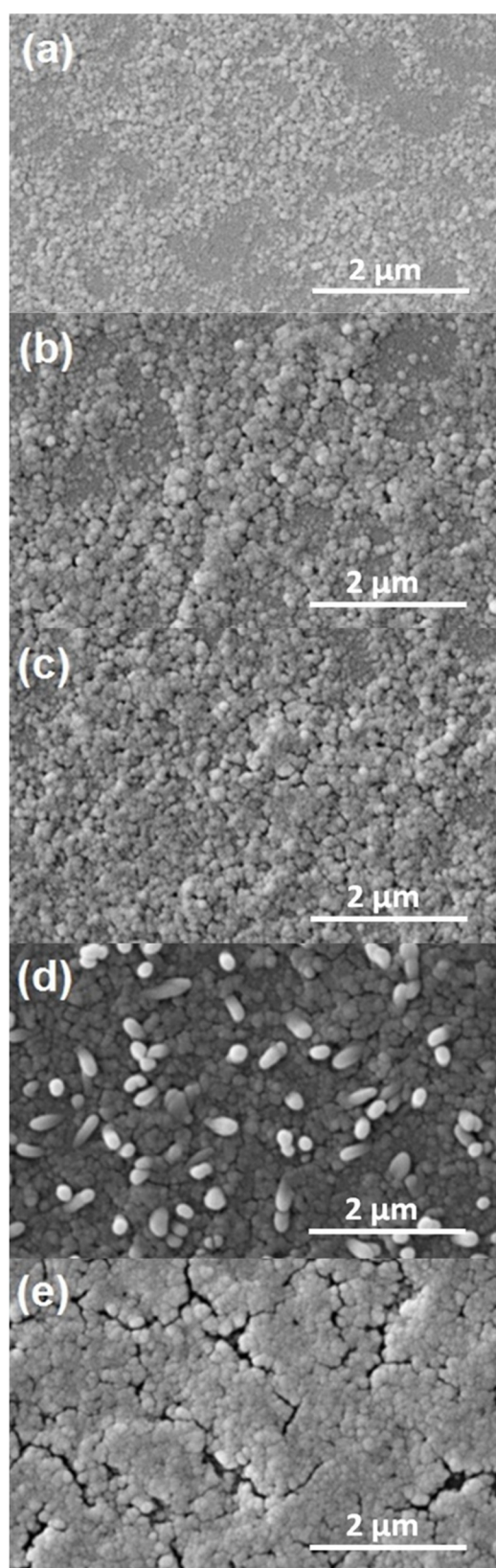
Figure 1. SEM images of the CdS sensitized titania films after (a) one, (b) two, (c) three, (d) four and (e) five SILAR cycles

After the fourth SILAR cycle, the previous porous layer turns into a compact layer, and some of the CdS particles grow preferentially on some points of the surface as a result of the deposition conditions. After the fifth SILAR cycle, a secondary layer with large, compact masses forms on the previous layer due to the extreme deposition of CdS particles.

3.2. Topography AFM's 3D topographies of the surface of the CdS sensitized titania films after different SILAR cycles are shown in Fig. 2. As it could be seen, all the samples present approximately a hill-valley like morphology. After the first two SILAR cycles, the surface topography is nonhomogeneous which is caused by the non-uniform size of particles and their dispersion. The surface topography becomes more homogeneous after the third SILAR cycle, which is due to the aggregation of particles and the formation of a layer. The root mean square (RMS) roughness after the first SILAR cycle is 8.5 nm, rising to 14.1 nm after the second cycle. However, the trend decreases as it continues and drops to 7.2 nm after the fifth SILAR cycle (as demonstrated in the table 1). The increase in the RMS roughness after the first two SILAR cycles is due to the increase in the number and size of the deposited particles, as it was observed in the SEM images. However, the decrease in the RMS roughness after the third SILAR cycle, although the particle sizes increase, is caused by the aggregation of particles and formation of a layer. The height difference between the hills and valleys of the surface decreases as the uniform CdS layer forms. Moreover, the difference further decreases as the pores disappear.

TABLE 1. Average and root mean square roughness of CdS sensitized titania films after different SILAR cycles

SILAR cycles	Average roughness (nm)	Root mean square roughness (nm)
1	6.8	8.5
2	11.1	14.1
3	9.6	12.2
4	7.2	9.1
5	5.8	7.2

3.3. Optical characterization The incorporated amount and the size distribution of CdS photosensitizers on titania films were evaluated using the absorbance of UV-Vis spectrum. Fig. 3a shows the absorbance spectra of the CdS sensitized titania films after different SILAR cycles. All the films exhibit low absorption in the visible region which is enhanced with their entrance to the ultraviolet region. By increasing SILAR cycles, the absorption of the films has a considerable enhancement in ultraviolet and visible

regions, which is due to the increase in the number of CdS particles formed on the titania films.
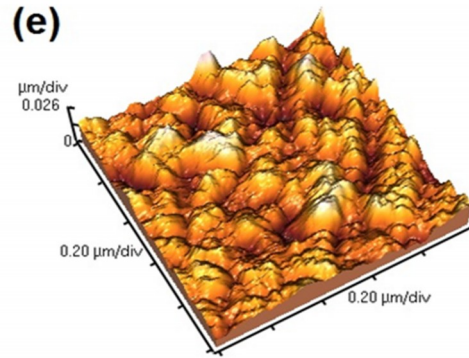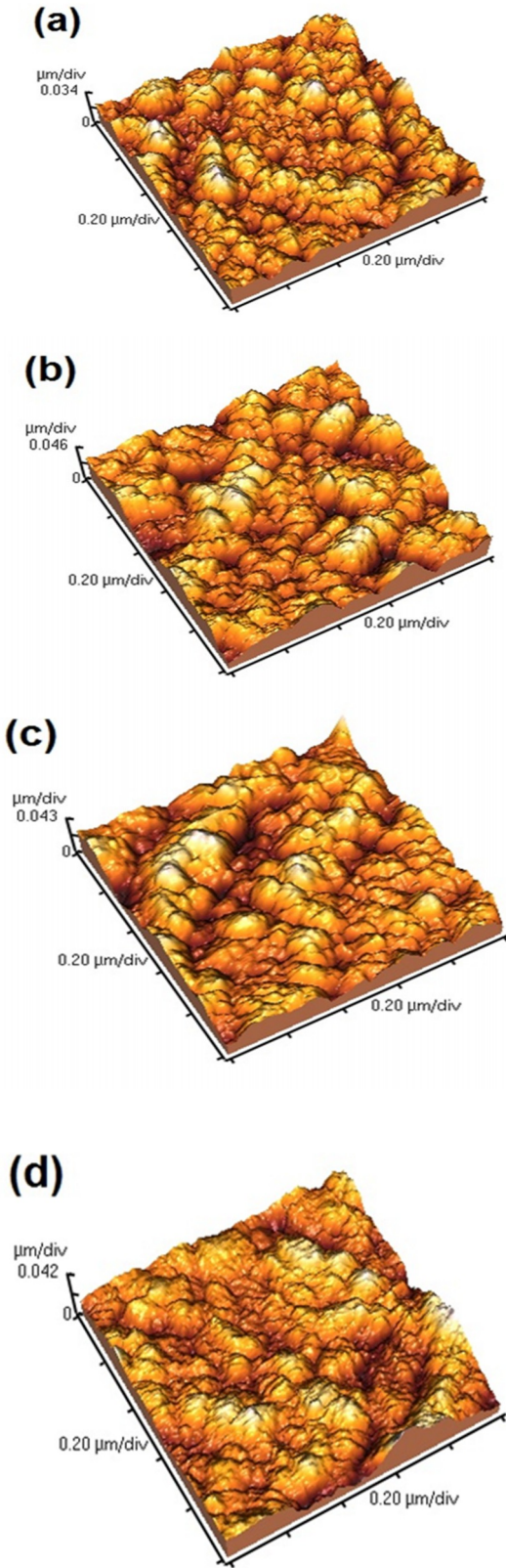

Figure 2. AFM images of the CdS sensitized titania films after (a) one, (b) two, (c) three, (d) four and (e) five SILAR cycles
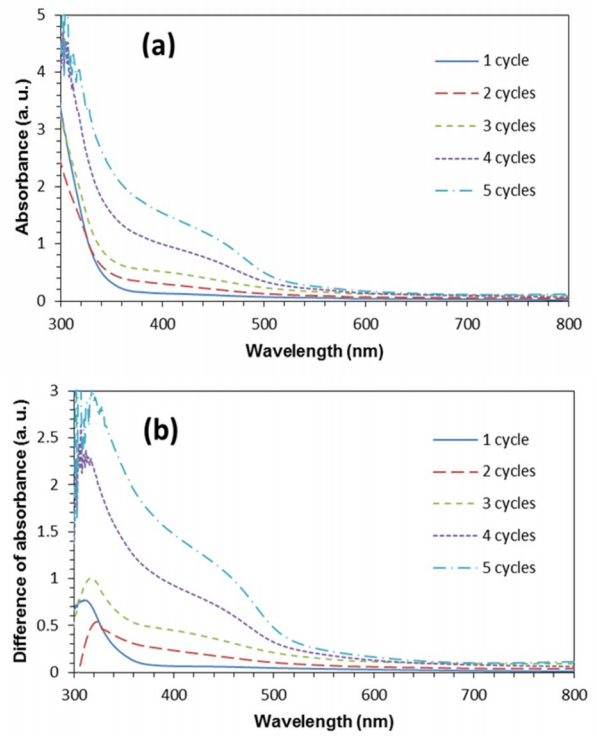

Figure 3. (a) Absorbance spectra of the CdS sensitized titania films, and (b) difference of absorbance of Titania films without and with CdS sensitization after different SILAR cycles

The absorption ranges of the films with CdS particles deposited on them starts from approximately 550 and 600 nm after the first two cycles and after cycles three to five, respectively. This shift is caused by the increase of the CdS particle size distributions. However, CdS nanoparticles could be considered as the secondary particles which have been formed by the aggregation of smaller quantum dots [19, 20].

The difference of the absorbance of titania films without and with CdS sensitization after different SILAR cycles are illustrated in Fig. 3b. The effect that the sensitization

of CdS photosensitizer leaves on the titania films could be easily noticed due to the difference of absorbance spectrum when a broad absorbance peak has been observed in ultraviolet and visible regions. This indicates that the CdS photosensitizers are more photoactive and mainly responsible for the electron generation in these regions. The difference of absorbance spectrum of CdS photosensitizer which is prepared after the fifth SILAR cycles shows a higher value than the samples of CdS photosensitizer which are prepared in the other SILAR cycles.

3.4. Photovoltaic performance

Fig. 4 shows the photocurrent density-voltage (J-V) characteristics of the photoelectrochemical cells made of CdS sensitized titania films after different SILAR cycles. In addition, the corresponding photovoltaic parameters, such as short circuit current (Jsc), open circuit voltage (Voc), fill factor (FF) and power conversion efficiency (η) are all summarized in Table 2. It could be observed that as the SILAR cycles proceed from one to three, the short circuit current increases up to 9.65 mA/cm^2, but then decreases to reach 7.32 mA/cm^2 after the fifth SILAR cycle. The open circuit voltage experiences slight variations. The power conversion efficiency changes in proportion with the short circuit current so that it reaches a maximum of 4.65 % after the third cycles, then drops to a minimum of 2.64 %. The changes in the power conversion efficiency of a cell are determined by the two opposing factors, i.e. the particles size distribution and their occupied area. As it was demonstrated in the absorption spectrum, the number of the deposited CdS particles and their size distribution increase as further SILAR cycles are introduced, resulting in the absorption of more incident photons and the increased light harvest efficiency of cell. On the other hand, as the number of the deposited CdS particles increase, the mesoporous titania film active area decreases, resulting in a decreased absorption of photons by dye molecules and/or directly by the titania film.
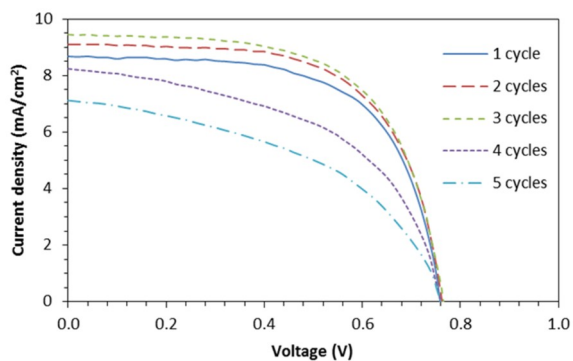

Figure 4. Photocurrent density-voltage curves of the photoelectrochemical cells made of CdS sensitized titania films after different SILAR cycles

TABLE 2. Photovoltaic parameters of the photoelectrochemical cells made of CdS sensitized titania films after different SILAR cycles

SILAR cycles	J_{SC} (mA/cm^2)	V_{OC} (V)	FF	η (%)
1	8.88	0.770	0.63	4.31
2	9.30	0.773	0.63	4.52
3	9.65	0.768	0.62	4.65
4	8.44	0.773	0.51	3.34
5	7.32	0.767	0.43	2.64

Additionally, charge exchange by the carriers weakens as the CdS nanoparticles block the electrolyte diffusion paths by their deposition on the titania film pores [17, 18].

The study of the cell intervals revealed that the increase in the number of particles as well as their size distribution up to the third SILAR cycle produced a dominant effect and increased the power conversion efficiency. However, in the fourth and fifth cycles, the effect of occupied area strongly increased so that the power conversion efficiency of the cell reached values lower than the initial efficiency.

4. CONCLUSION

In order to examine the effect of particles size distribution and their occupied surface area, photoelectrochemical cells were prepared using CdS photosensitizers as well as mesoporous titania films. SILAR method was used for an accurate control of nucleation process and CdS particles growth. Investigating the surface morphology using SEM revealed that after the initial SILAR cycles, some clusters of CdS particles were non-uniformly formed on the surface, through the growth and aggregation of which the compact layer forms.

The AFM images demonstrated that surface roughness decreased as the particles morphology of the surface turned into layered morphology.

The absorbance spectra measured by UV-Vis spectrophotometer revealed that the absorbance spectra increased and its limits shifted towards longer wavelengths as the number and size of particles increased. The maximum cell efficiency 4.65 % was achieved after the third SILAR cycle, which was due to the dominant effect of particles size distribution over their occupied surface area.

5. ACKNOWLEDGMENTS

REFERENCES

1. Yamaguchi, M., "II–V compound multi-junction solar cells: present and future", *Solar Energy Materials & Solar Cells,* Vol. 75, (2003), 261–269.

2. Xing, Y., Han, P., Wang, S., Fan, Y., Liang, P., Ye, Z., Li, X., Hu, S., Lou, S., Zhao, C. and Mi, Y., "Performance analysis of vertical multi-junction solar cell with front surface diffusion for high concentration", *Solar Energy,* Vol. 94, (2013), 8–18.

3. Patra, J.C. and Maskell, D.L., "Modeling of multi- junction solar cells for estimation of EQE under influence of charged particles using artificial neural networks", *Renewable Energy,* Vol. 44, (2012), 7-16.

4. Tzeng, W.J., Wu, M.L., Lin, L.J. and Chang, H.Y., "Chalcogenide photosensitized titania nanotube arrays", *Journal of Alloys and Compounds,* Vol. 651, (2015), 483-489.

5. Yilmaz, C. and Unal, U., "Photoelectrochemical properties of electrochemically deposited metal chalcogenide/ZnO films", *Applied Surface Science,* Vol. 350, (2015), 87–93.

6. Zou, J.P., Lei, S.L., Yu, J., Luo, S.L., Luo, X.B., Tang, X.H., Dai, W.L., Sun, J., Guo, G.C. and Au, C.T., "Highly efficient and stable hydrogen evolution from water with CdS as photosensitizer-A noble-metal-free system", *Applied Catalysis B: Environmental,* Vol. 150–151, (2014), 466– 471.

7. Prabakar, K., Seo, H., Son, M. and Kim, H., "CdS quantum dots sensitized TiO$_2$ photoelectrodes", *Materials Chemistry and Physics,* Vol. 117, (2009), 26-28.

8. Sudhagar, P., Jung, J.H., Park, S., Sathyamoorthy, R., Ahn, H. and Kang, Y.S., "Self-assembled CdS quantum dots-sensitized TiO$_2$ nanospheroidal solar cells: Structural and charge transport analysis", *Electrochimica Acta,* Vol. 55, (2009), 113-117.

9. Lee, W., Min, S.K. Dhas, V. Ogale, S.B. and Han, S.H., "Chemical bath deposition of CdS quantum dots on vertically aligned ZnO nanorods for quantum dots-sensitized solar cells", *Electrochemistry Communications,* Vol. 11, (2009),103-106.

10. Chen, H., Li, W., Liu, H. and Zhu, L., "A suitable deposition method of CdS for high performance CdS-sensitized ZnO electrodes: Sequential chemical bath deposition", *Solar Energy,* Vol. 84, (2010), 1201-1207.

11. Hernandez-Pereza, M.A., Aguilar-Hernandez, J., Contreras-Puente, G., Vargas-Garcia, J.R. and Rangel-Salinas, E., "Comparative optical and structural studies of CdSe films grown by chemical bath deposition and pulsed laser deposition", *Physica E,* Vol. 40, (2008), 2535-2539.

12. Shen, Q., Yanai, M., Katayama, K., Sawada, T. and Toyoda, T., "Optical absorption, photosensitization, and ultrafast carrier dynamic investigations of CdSe quantum dots grafted onto nanostructured SnO$_2$ electrode and fluorine-doped tin oxide (FTO) glass", *Chemical Physics Letters,* Vol. 442, (2007), 89-96.

13. Fan, S.Q., Kim, D., Kim, J.J., Jung, D.W., Kang, S.O. and Ko, J., "Highly efficient CdSe quantum dot sensitized TiO$_2$ photoelectrodes for solar cell applications", *Electrochemistry Communications,* Vol. 11, (2009), 1337-1339.

14. Mali, S.S., Desai, S.K., Dalavi, D.S., Betty, C.A., Bhosalea, P.N. and Patil, P.S., "CdS-sensitized TiO$_2$ nanocorals: hydrothermal synthesis, characterization, application", *Photochemical & Photobiological Sciences,* Vol. 10, (2011), 1652-1658.

15. Zhang, Q., Cao, J. and Li, H., "CdS sensitized TiO$_2$ photoanodes for quantum dot-sensitized solar cells by hydrothermal assisted chemical bath deposition and post-annealing treatment", *RSC Advances,* Vol. 5, (2015), 107957-107963.

16. Chong, L.W., Chien, H.T. and Lee, Y.L., "Assembly of CdSe onto mesoporous TiO$_2$ films induced by a self-assembled monolayer for quantum dot-sensitized solar cell applications", *Journal of Power Sources,* Vol. 195, (2010), 5109-5113.

17. Zhang, Y., Zhu, J. Yu, X., Wei, J., Hu, L. and Dai, S., "The optical and electrochemical properties of CdS/CdSe co-sensitized TiO$_2$ solar cells prepared by successive ionic layer adsorption and reaction processes", *Solar Energy,* Vol. 86, (2012), 964-971.

18. Lee, W., Kwak, W.C., Min, S.K., Lee, J.C., Chae, W.S., Sung, Y.M. and Han, S.H., "Spectral broadening in quantum dots-sensitized photoelectrochemical solar cells based on CdSe and Mg-doped CdSe nanocrystals", *Electrochemistry Communications,* Vol. 10, (2008), 1699-1702.

19. Rawal, S.B., Sung, S.D., Moon, S.Y., Shin, Y.J. and Lee, W.I., "Optimization of CdS layer on ZnO nanorod arrays for efficient CdS/CdSe co-sensitized solar cell", *Materials Letters,* Vol. 82, (2012), 240-243.

20. Deng, J., Wang, M., Song, X., Shi, Y. and Zhang, X., "CdS and CdSe quantum dots subsectionally sensitized solar cells using a novel double-layer ZnO nanorod arrays", *Journal of Colloid and Interface Science,* Vol. 388, (2012), 118-122.